Applied Catalysis B: Environmental 202 (2017) 207–216

Contents lists available at ScienceDirect

Applied Catalysis B: Environmental

journal homepage: www.elsevier.com/locate/apcatb

Dehalogenation of aromatic halides by polyaniline/zero-valent iron composite nanofiber: Kinetics and mechanisms

Somnath Giri[a], Madhumita Bhaumik[b], Raghunath Das[a], Vinod Kumar Gupta[b], Arjun Maity[a,c,*]

[a] Department of Chemical Engineering, University of South Africa, Muckleunek 0003, South Africa
[b] Department of Applied Chemistry, University of Johannesburg, Johannesburg, South Africa
[c] National Centre for Nanostructured Materials, Materials Science and Manufacturing, Council for Scientific and Industrial Research (CSIR), Pretoria, South Africa

ARTICLE INFO

Article history:
Received 7 June 2016
Received in revised form 21 August 2016
Accepted 13 September 2016
Available online 13 September 2016

Keywords:
Reductive dehalogenation
Aryl halides
PANI/Fe^0 composite nanofibers
Grignard reagents
Heterogeneous catalyst

ABSTRACT

Dehalogenation of aryl halides was demonstrated using polyaniline/zero valent iron composite nanofiber (termed as PANI/Fe^0) as a cheap, efficient and environmentally friendly heterogeneous catalyst. The catalyst was prepared via rapid mixing polymerization of aniline monomers with Fe(III) chloride as an oxidant followed by reductive deposition of nano-sized Fe^0 onto the PANI nanofiber using the by-products (Fe(II)/Fe(III)) present in the polymerization system as the Fe precursor. The catalyst was characterized by various physico-chemical techniques: ATR-FTIR, FE-SEM, HR-TEM, XRD, XPS and VSM. A mild reductive dehalogenation process of a wide range of aromatic bromides was explored in the presence of PANI/Fe^0 catalyst. The catalyst was active and manifested a high reactivity (84% GC yield of naphthalene for 7 h at 40 °C) with four equivalents of *t*-BuMgCl. Deiodination reaction was proved to be more facile in comparison with their corresponding halides. Kinetic studies at different temperatures (30, 40, 50, and 60 °C) revealed an overall pseudo-first-order behaviour with rate constants 0.00281, 0.00893, 0.01137 and 0.02421 min^{-1}, respectively. The reaction profile diagram of substrate consumption and the product formation rate indicated that there is no additional induction period was involved in the catalytic cycle. Activation energy (E_a) was calculated to be 56.3 kJ/mol through Arrhenius plot. Several deuteration experiments were conducted with different Grignard reagents to understand the mechanism of the reaction. These studies explained that the hydride incorporated product was obtained through β-hydride elimination of *t*-BuMgCl. The catalyst was tested up to three cycles whereas the full conversion of the product was obtained for a prolonged period. PANI/Fe^0 could be an alternative suitable catalyst for dehalogenation of environmentally poisonous aromatic halides.

1. Introduction

Halogenated organic compounds (HOCs) are mostly ubiquitous non-biodegradable pollutants in the environment [1–3]. A large number of HOCs are extensively used in chemical industry [1–3], and also naturally produced [4,5]. Typically, the majority of pernicious brominated compounds, due to their persistence and flame retardants in nature, are easily contaminated and often bioaccumulated in the food chain [1–3,6,7]. For the remediation of HOCs, it is very important to investigate the effective chemical process for the reclamation of hazards organic halides to less toxic hydrocarbon compounds, and to diminish the resistant waste in our eco-system.

In recent years, a considerable amount of work has been reported for dehalogenation of organic halides e.g. photochemical [8,9], oxidation [10,11], and biological processes [12,13]. Metal-catalyzed reductive dehalogenation is one of the most efficient and well-known alternative method in organic synthesis with various available hydrogen sources. For examples, several methods have been performed with highly expensive, toxic metals (*e.g.* Ni, Pd, Rh, Ru), as well as environmentally noxious reductants (*e.g.* Bu_3SnH, formate, N_2H_4, $NaBH_4$, Et_3SiH, Zn, H_2 gas, etc) [14–26]. Therefore, the development of cost effective, and practical catalytic methods are needed to be explored using cheap, and readily available reductant in combination with less toxic, and less expensive metal

* Corresponding author at: National Centre for Nanostructured Materials, Materials Science and Manufacturing, Council for Scientific and Industrial Research (CSIR), Pretoria, South Africa.
E-mail addresses: maityarjun@gmail.com, amaity@csir.co.za (A. Maity).

http://dx.doi.org/10.1016/j.apcatb.2016.09.027
0926-3373/

catalysts. Consequently, several research groups have been investigated the dehalogenation methods by employing iron as a catalyst [27–30]. However, iron-catalyzed dehalogenation is still to be a demanding task, owing to the issues of environment concern, as well as cost effectiveness of the catalyst.

The use of heterogeneous catalyst has aroused a lots of attention compared to homogeneous catalyst with regard to catalyst stability, handling and recyclability [31,32]. In recent years, nanosize metal catalysts are powerful effective tools in the catalytic organic transformation reactions [33–35]. However, the catalyst incorporated with nanofiber supported matrix enhances excellent recycling efficiency [36]. In the development of sustainable catalyst [37], current research trends have fascinated ample attention to find out alternative ways by using cheap, large-abundant, and non-toxic supported metal catalyst. On that note, iron-based nanomaterials are generally recovered from the reaction mixture through simple magnetic separation [38,39]. It is noteworthy that all these properties of iron based magnetic nanoparticles offer unique advantages over their inorganic salts and complexes [40,41].

Furthermore, PANI/Fe^0 or Fe_3O_4 nanocomposite particles, due to its high surface area, have found potential application in water treatment [42–46], corrosion resistance [47,48], fuel cell [49–51], electronic device manipulation [52,53], sensor [54,55], and fabrication [56]. Recently, Fe-PANI/SiO_2 core-shell supported metal nanoparticles have shown their catalytic efficiency and recyclability in organic synthesis [57]. Bhaumik et al. reported that PANI/Fe^0 nanofibers could be used for the removal of Cr(VI), As(V) and Congo red (CR) dye [44–46]. The kinetics result followed the pseudo-second-order model whereas isotherm results fitted well with Langmuir model. The following two mechanisms for the removal of As(V) were proposed: (i) the adsorption process and (ii) the substitution of surface bonded OH^- ligands produced by the reaction of Fe^0 and H_2O/O_2, whereas both adsorption and reduction mechanisms associated with the removal of Cr(VI). For CR dye removal, the degradation mechanism involved through reductive cleavage of the azo linkage of dye by nano-Fe^0[46]. Haspulat et al. [43] disclosed the photocatalytic degradation mechanism for the decolourization of textile dyes using Fe ions doped PANI film, whereas Yue et al. [42] explained that the oxidation degradation process involved for the removal of Rhodamine B. Bhaumik et al. [45] also investigated the adsorption behaviour using PANI nanofibers as a highly effective reusable adsorbent. The kinetic data fitted well with pseudo-second-order and adsorption mechanism involved the ionic interaction between positive charge adsorbents and negative charge dye. However, to the best of our knowledge, no scientific study has been reported on the catalytic reactivity of PANI/Fe^0 composite nanofibers material for the dehalogenation of aryl halides in the literature. Hence, iron(0)-catalyzed transformations are still to be established for further applications in catalysis. This interest prompted our search to explore whether iron(0) decorated PANI nanofibers would be a potential recyclable catalyst for reductive dehalogenation of aryl halides.

As part of our current efforts aimed at developing the economical metal nanomaterials [45,58], herein, we report these findings for reductive dehalogenation of aromatic halides using PANI/Fe^0 composite nanofibers. In this work, PANI/Fe^0 composite nanofibers, heterogeneous catalyst, were prepared via reductive deposition of nano-sized Fe^0 onto the PANI nanofibers matrix for the dehalogenation of aromatic halides. The catalytic activity was tested on different Fe^0 loading catalyst, substrates, time and temperature. The leaching and reusability tests were also conducted to know the feasibility of the catalyst. Finally, a plausible mechanism was established for the catalytic cycle.

2. Experimental

2.1. Chemicals

Aniline (ANI, 99%) monomer, anhydrous iron (III) chloride ($FeCl_3$) and sodium borohydride ($NaBH_4$) were purchased from Sigma-Aldrich, USA. The monomer was purified by vacuum distillation prior to use and kept in the refrigerator. Ultrapure water was collected from an EASY pure® II, UV-ultrapure water system, for the preparation of catalyst and for the preparation of all experimental solutions. Aryl halides, Grignard reagents and Bromoethane-2,2,2-D_3 were bought from Sigma-Aldrich, USA. All other chemicals used were of reagent grade. All solvents used were dried according to the standard procedures for the catalytic experiment.

2.2. Preparation of catalyst

The catalyst, PANI/Fe^0 composite nanofiber with different Fe^0 loadings, was prepared using our previously reported method [44,58]. Firstly, the PANI nanofibers (PANI NFs) were prepared by rapid mixing technique using $FeCl_3$ as an oxidant at room temperature. In briefly, 0.8 mL of ANI monomer was syringed rapidly in 80 mL of anhydrous $FeCl_3$ solution in a 250 mL conical flask. The reaction mixture was stirred for 5 min to evenly distribute the oxidant and monomers to prevent the secondary growth of the polymer. Then, the reaction mixture was kept without stirring for 2 days and followed by filtered, washed with water and acetone, and finally dried at 60 °C.

Secondly, to support the Fe^0, the prepared PANI nanofibers were used as support without removing them from the polymerization medium and polymerization by-products ($FeCl_2$ and/or any remaining $FeCl_3$) as the source of Fe^0. To prepare PANI/Fe^0 composite nanofibers, a freshly prepared sodium borohydride ($NaBH_4$) solution (100 mL) was added dropwise to the PANI-polymerization system by mechanical stirring under a N_2 atmosphere for 10 min. The reaction mixture was stirred for another 20 min and the product (PANI/Fe^0) was filtered, washed with water and ethanol and dried at 60 °C. To know the content of Fe^0 in the composite, leached solution (con. HCl) was analysed using ICP-OES technique and it was found to be 4.9% Fe^0 loading in the composite. To prepare other compositions of Fe^0 loading the same preparative methods were conducted using different concentrations of $NaBH_4$ solution. From now, we have labelled the catalyst as follows: PANI/Fe^0-1(1.02%), PANI/Fe^0-2(4.9%), PANI/Fe^0-3(9.97%), PANI/Fe^0-1(30.10%) and PANI/Fe^0-1(70.06%). For catalytic activity test, it was found that PANI/Fe^0-2 catalyst was performed better than other compositions. Therefore, PANI/Fe^0-2 catalyst was selected for different characterizations.

2.3. Characterization

The morphology and size of the PANI and PANI/Fe^0-2 were investigated by an Auriga Field Emission Scanning Electron Microscope (FE-SEM; Carl Zeiss, Germany) and a JEOL JEM-2100 High Resolution Transmission Electron Microscope (HR-TEM; JEOL, Japan). A JEOL JEM-2100 HR-TEM instrument with a LaB6 filament operated at 200 kV was used to obtain TEM images. Specimen for HR-TEM was prepared by placing a drop of a dilute suspension of the sample in 2-propanol on a copper grid. X-ray diffraction (XRD) pattern of the PANI/Fe^0-2 was performed using an X-ray powder diffractometer with Cu anode (PANalytical Co. X'pert PRO, UK), running at 40 kV and 30 mA, scanning from 10° to 80° with a scan speed of 1°/min. An Attenuated Total Reflectance-Fourier Transform Infrared (ATR-FTIR) Spectrum 100 Spectrometer (Perkin-Elmer, USA), with a germanium crystal was employed to record the IR spectrum of the PANI/Fe^0-2. For the IR mea-

surement, the frequency range, resolution and number of scans were 600–2000 cm^{-1}, 4 cm^{-1} and 10 cm^{-1}, respectively. Elemental mapping and oxidation states of the elements of the PANI/Fe^0-2 were obtained using X-ray photoelectron spectroscopy (XPS) on a Kratos Axis Ultra device, with an Al monochromatic X-ray source (1486.6 eV). XPS curve fitting and background subtraction were accomplished using XPS PEAK 41 software. For analysis of Fe content in the PANI/Fe^0, the PANI/Fe^0 was digested with 2 M HCl. The filtrate was used to determine Fe content using an inductively coupled plasma-optical emission spectrometer (ICP-OES, Spectro-Arcos, Germany). Analytical thin layer chromatography was performed on aluminum sheets (Kieselgel 60 F-254) for catalytic reaction. Dehalogenated products were isolated by column chromatography on 100–200 mesh silica gels by using ethyl acetate (EtOAc)/hexane as eluent. GC analyses were performed with Agilent 7890A gas chromatograph. ^1H NMR and ^{13}C NMR spectra were recorded on a Varian 400 MHz INOVA system running VNMRJ 4.2A software using a 55 mm indirect detection pulsed field gradient room temperature probe operates at 30 °C. Chemical shift values (δ) for protons and carbon atoms were expressed in parts per million (ppm) with respect to TMS. $CDCl_3$ was used as solvent for NMR spectra.

2.4. Catalytic experiment

1-Bromonaphthalene (1 mmol, 207 mg), PANI/Fe^0-2 (2.5 mol%, 28.6 mg), and dry toluene (2 mL) were added in an oven-dried Schlenk tube under N_2 atmosphere. Then, 4 mL of 1(N) *t*-BuMgCl was added drop wise to the reaction mixture at room temperature. The resulting mixture was stirred at 40 °C for 7 h, and then quenched with saturated NH_4Cl (2 mL) at 0 °C. The reaction mixture was extracted three times with EtOAc (20 mL) and combined organic layer was dried over anhydrous $MgSO_4$. The crude product was purified by column chromatography on silica gel (100–200 mesh) using hexane as eluent to furnish naphthalene as pure product. The purity of naphthalene was analysed by Gas chromatogram, ^1H NMR and ^{13}C NMR spectroscopy.

3. Results and discussion

3.1. Characterization of the catalyst

An ATR-FTIR spectrum of the PANI/Fe^0-2 catalyst showed the bands at 1576, 1495, 1285, 1216, 1173 and 815 cm^{-1} which are assigned to the stretching vibrations of quinonoide (Q), benzenoid (B) rings, C—N vibrational frequencies in Q-B-Q, C—N vibrational frequencies in B unites, B-NH^+ = Q stretching and aromatic C—H deformation vibrations of linear PANI backbone, respectively [59,60]. These features indicated the presence of PANI moieties in the PANI/Fe^0-2 catalyst.

The SEM images of (a) PANI NFs, and (b) PANI/Fe^0-2 catalyst are presented in Fig. 1. It was observed from Fig. 1a that the as-prepared PANI NFs have a smooth surface with diameter 50–80 nm. It was interesting to note that after the incorporation of Fe^0 nanoparticles, the diameters of the PANI NFs are increased between 70 and 140 nm (Fig. 1b) and have a rougher surface than pure PANI NFs. TEM images of the prepared PANI/Fe^0-2 catalyst at two different magnifications are depicted in Fig. 2. It showed that the PANI/Fe^0 is branched like structure and a closer observation of PANI/Fe^0 revealed that Fe^0 with various size distributions are facilely deposited onto PANI NFs matrix. The STEM (Fig. 2d) image also represented the distribution of Fe^0 nanoparticles onto the PANI networks.

Fig. 3a illustrates the X-ray diffraction (XRD) pattern of the PANI/Fe^0-2 catalyst. It can be seen from Fig. 3a that two peaks

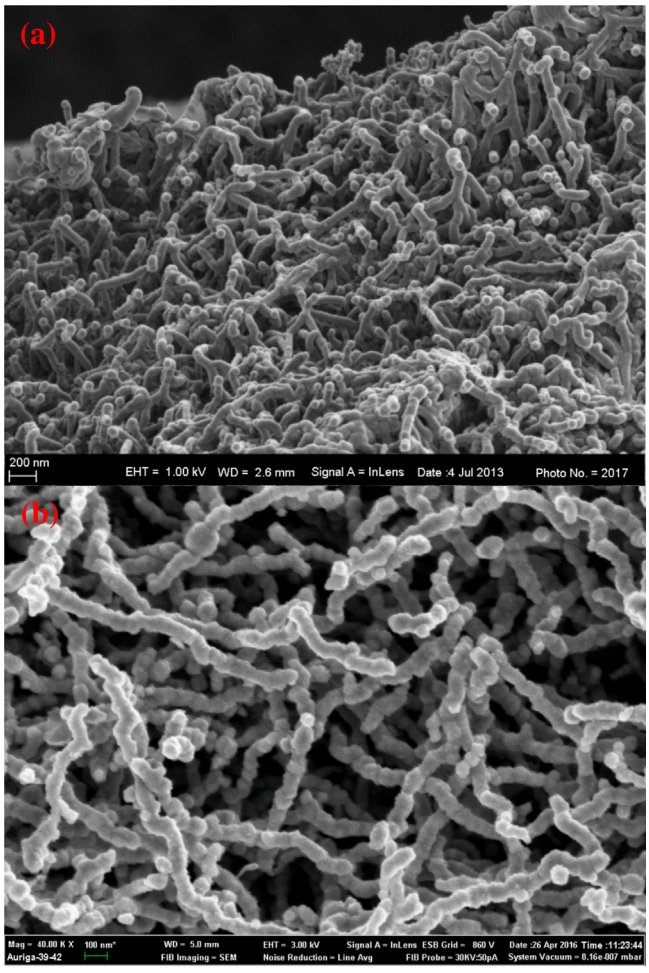

Fig. 1. SEM images of (a) PANI nanofibers and (b) PANI/Fe^0-2 catalyst.

were observed, at 2θ, of 44.79° and 65.15°, which are in good agreement with the (200) and (110) planes of Fe^0 nanoparticles, respectively [61,62]. The average grain size of the supported Fe^0 particles was found to be 14.17 nm calculated from the broadening of the (110) diffraction peak using the Scherrer's equation. The broad band centred at 2θ = 20.34° confirmed the amorphous feature of PANI NFs. This implied that Fe^0 nanoparticles are successfully embedded/deposited on the PANI matrix.

In order to analyze the content and chemical state of the N and Fe in the PANI/Fe^0-2 catalyst, X-ray photoelectron spectroscopy (XPS) analysis was done. It can be observed from the survey scan of the catalyst (Fig. 3a) that the presence of Fe 2p peak confirmed the successful incorporation of Fe^0 nanoparticles into the PANI matrix. The core level spectrum of Fe 2p is also presented in Fig. 3b. The Fe 2p spectrum could also be deconvoluted into peaks centred at 710.45 eV and 712.62 eV corresponding to the binding energies of Fe 2p3/2, while peaks centred at 722.08 eV, 724.28 eV are associated with Fe 2p1/2 binding energies [63]. The observed Fe 2p peaks are in conformity with FeO, FeOOH and Fe_3O_4, which suggests that Fe^0 nanoparticles deposited onto PANI matrix were enclosed by a thin layer of iron oxides [64]. In addition a very weak satellite peak at 706.36 eV corresponding to Fe^0 2p3/2 was barely detectable due to the high surface sensitivity (less than 10 nm in depth) of XPS.

Fig. 3d represents the room temperature magnetic hysteresis loop of the PANI/Fe^0-2 catalyst. It was noted that the nonlinear hysteresis loops with saturation magnetization (Ms) of ~22.1 emu/g and nonzero remnant magnetization (Mr) demonstrated well pronounced ferromagnetic property of the catalyst. This indicated the

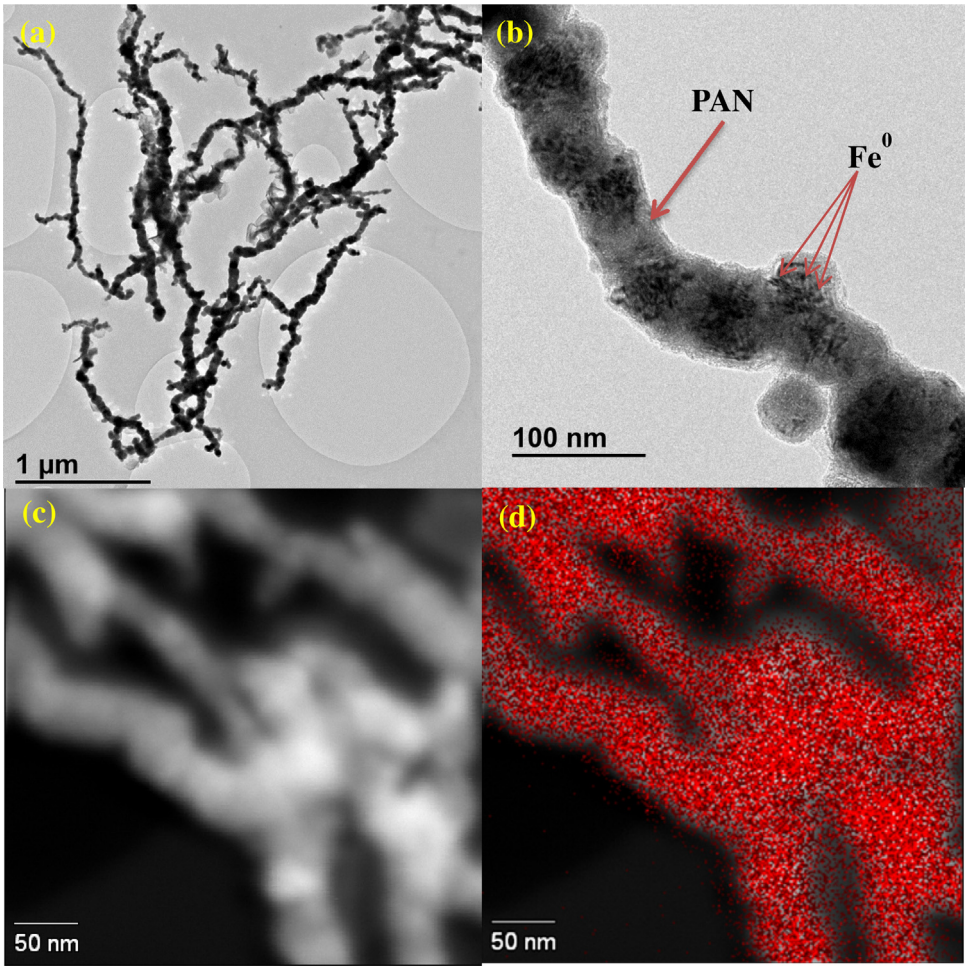

Fig. 2. TEM images of the PANI/Fe^0-2 catalyst at two different magnifications (a, b) and (c) STEM image of the PANI/Fe^0-2 catalyst, and (d) chemical mappings of iron.

easy separation of the catalyst after completion of the chemical transformation from the reaction vessel by applying magnetic field.

3.2. Performance of the catalyst in different conditions

In the initial stage of the work, we commenced our investigation to explore the dehalogenation reaction of 1-bromonaphthalene **(1)** with Grignard reagents **(2)**, as summarized in Table 1. To check the effect of Fe^0 loading in the catalyst for catalysis reaction, we have studied with EtMgBr under different PANI/Fe^0 catalysts (see SI) and PANI/Fe^0-2 was found to be effective furnishing the desired product, naphthalene **(1a)**, in 77% GC yield (Table 1, entry 1).

However, a minor amount of cross-coupling product (<15%) was formed with EtMgBr as a side product. To suppress cross-coupling product, further studies were carried out with different alkyl Grignard reagents (Table 1, entries 2 and 3). These studies revealed that *t*-BuMgCl was able to furnish the desired product in 58% yield (Table 1, entry 3) where no cross-coupled product was obtained (Table 1, entry 3). However, lowering the temperature to 25 °C did not improve the yield of the reductive product (Table 1, entry 4). To enhance the efficiency of the catalytic system, the reaction was optimized with various solvents (Table 1, entries 5 and 6). This study indicated that toluene was found to be the best counterpart solvent with tetrahydrofuran (1:2). Herein, we mentioned that no additional THF was used in this catalytic condition. These attempts furnished conversion up to 71% yield of product at 40 °C for 5 h in toluene. This study encouraged us for further investigation to evolve the most suitable reaction condition. At this stage, the dehalogenation reactions were performed for 6 h and 7 h to furnish the corresponding product in 76% and 84% GC yields, respectively (Table 1, entries 7 and 8). Notably, this effort decided that 7 h reaction time was sufficient for completion of the reaction with high product yield (Table 1, entry 8). Under similar condition, the reaction was conducted at 30 °C which did not improve the yield of the product (Table 1, entry 9). Further, it was of interest to check reactions with 2 equiv. and 3 equiv. of *t*-BuMgCl provided only 47% and 63% yield, respectively (Table 1, entries 10 and 11). Hence, it was decided to continue the studies with 4 equiv. of the *t*-BuMgCl to drive the reaction towards dehalogenation with the suppression of the competitive cross-coupling process. However, 1.5 mol% loading of catalyst afforded only 55% yield of the product (Table 1, entry 12). Expectedly, additional two control reactions were performed without *t*-BuMgCl and catalyst furnished poor (<10%) and no conversion, respectively (Table 1, entries 13 and 14). From our optimization study, the dehalogenation reaction was established using PANI/Fe^0-2 (2.5 mol%) as catalyst and *t*-BuMgCl (4equiv.) as reductant in toluene solvent to give high yield of product at 40 °C for 7 h reaction time (Table 1, entry 8).

Hence, this effort prompted to check further scope of the reaction with a variety of electron rich and electron deficient aryl halides under optimized reaction condition, as summarized in Table 2 . It is noteworthy that 1-bromonaphthalene and 1-bromo-6-methoxynaphthalene afforded the desired product in excellent isolated yield (Table 2, entries 1 and 2). However, *electron-poor* substrates such as 4-bromobenzotrifluoride, 1-bromo-4-nitrobenzene were found to be facile with high product yields, while the cor-

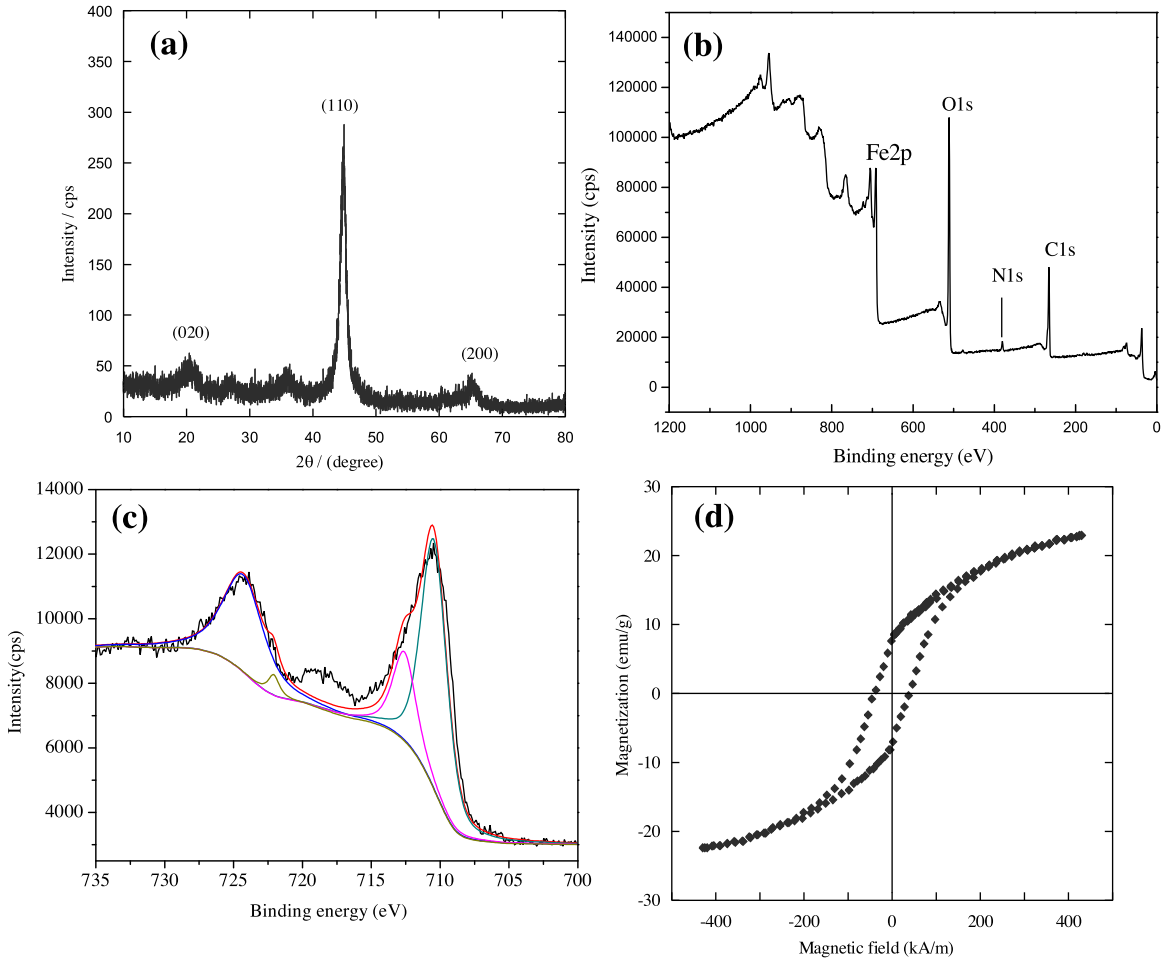

Fig. 3. (a) XRD pattern of the PANI/Fe^0-2 catalyst, (b) XPS survey scan of PANI/Fe^0-2 catalyst, (c) Fe 2p XPS spectrum of the PANI/Fe^0-2 catalyst and (d) Room temperature hysteresis loop of the PANI/Fe^0-2 catalyst.

Table 1
Screening conditions.[a]

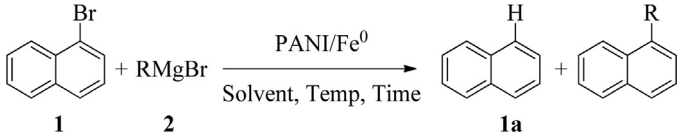

Entry	Catalyst	RMgX	Solvent	Temp (°C)	Time (h)	Yield (%)[b]
1	PANI/Fe^0−2[h]	EtMgBr	THF	40	5	77 (<15)
2	PANI/Fe^0−2[h]	*i*-PrMgBr	THF	40	5	30
3	PANI/Fe^0−2[h]	*t*-BuMgCl	THF	40	5	58(0)
4	PANI/Fe^0−2[h]	*t*-BuMgCl	THF	25	5	21(0)
5	PANI/Fe^0−2[h]	*t*-BuMgCl	toluene	40	5	71(0)
6	PANI/Fe^0−2[h]	*t*-BuMgCl	DMF	40	5	27(0)
7	PANI/Fe^0−2[h]	*t*-BuMgCl	toluene	40	6	76(0)
8	PANI/Fe^0−2[h]	*t*-BuMgCl	toluene	40	7	84 (0)
9	PANI/Fe^0−2[h]	*t*-BuMgCl	toluene	30	7	68 (0)
10[c]	PANI/Fe^0−2[h]	*t*-BuMgCl	toluene	40	7	47 (0)
11[d]	PANI/Fe^0−2[h]	*t*-BuMgCl	toluene	40	7	63 (0)
12[e]	PANI/Fe^0−2[h]	*t*-BuMgCl	toluene	40	7	55 (0)
13[f]	PANI/Fe^0−2[h]	none	toluene	40	7	0
14[g]	none	*t*-BuMgCl	toluene	40	7	(<10)

[a] Reaction Condition:1-bromonaphthalene (1 mmol), solvent (2 mL), catalyst (2.5 mol%), RMgX (4 equiv.).
[b] Yields measured by GLC analysis of the crude reaction mixture using undecane as internal standard. GC conversion of cross-coupling product shown in parentheses.
[c] With *t*-BuMgCl (2 equiv.).
[d] With *t*-BuMgCl (3 equiv.).
[e] Catalyst (1.5 mol%).
[f] Control without *t*-BuMgCl.
[g] Control without catalyst, GC conversion shown in parentheses.
[h] PANI/Fe^0-2 catalyst (4.9% Fe).

Table 2
Dehalogenation of Aryl halides with *t*-BuMgCl.[a]

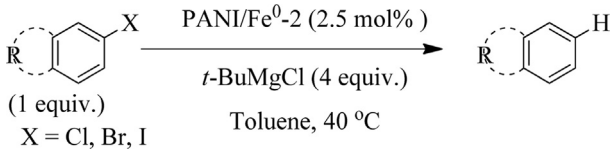

Entry	Substrate	Product	Time (h)	Yield (%)[b]
1.		 **1a**	7	78
2.	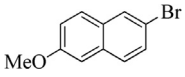	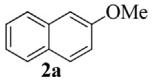 **2a**	5	82
3.	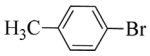	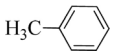	9	72[c]
4.	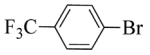	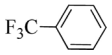	6	81[c]
5.	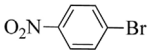	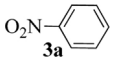 **3a**	5	85
6.	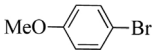	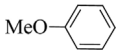	16	65[c]
7.	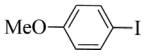	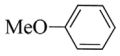	8	74[c]
8.	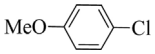	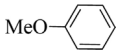	24	56[c]
9.	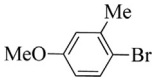	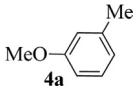 **4a**	12	58
10.	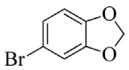	 **5a**	12	61
11.	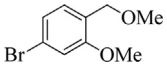	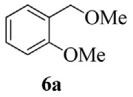 **6a**	16	71
12.	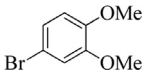	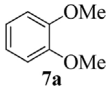 **7a**	18	68
13.	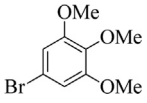	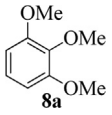 **8a**	48	67
14.	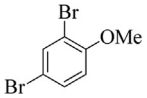	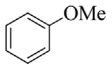	24	52[c,d]

[a] Reaction condition: Aryl halide (1 mmol), toluene (2 mL), PANI/Fe^0-2 (2.5 mol%), 40 °C, *t*-BuMgCl (4 equiv.).
[b] Isolated yield.
[c] Yields measured by GLC analysis of the crude reaction mixture using undecane as internal standard.
[d] With *t*-BuMgCl (8 equiv.).

responding dehalogenation reaction with *electron-donating* aryl bromides furnished moderate yields (Table 2, entries 3–6). To check the efficiency among the halides, 4-iodoanisole was proved to be more efficient in oxidative addition compared to 4-bromo- and 4-chloroanisole (Table 2, entries 6–8). Notably, the catalytic reactivity of 1-bromo-2-methylanisole was taken longer reaction period with 58% yield of the product (Table 2, entry 9). The fact could be explained by steric imposed due to the presence of methyl group at *ortho* position. Additional studies were checked with highly *electron-rich* functionalized aryl bromides under standard reaction protocol. It is interested to note that all these reactions afforded the corresponding dehalogenation product with moderate to good yields in longer reaction time (Table 2, entries 10–13). The dehalogenation reaction was further tested with 2,4-dibromoanisole obtaining the corresponding reduction product in 52% yield (Table 2, entry 14).

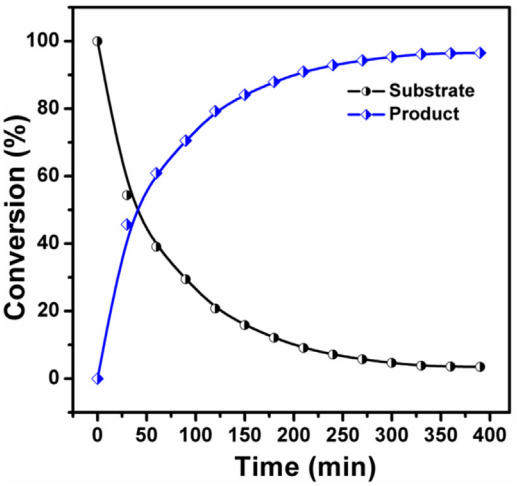

Fig. 4. Time-conversion plot of **1** catalyzed by PANI/Fe^0-2 catalyst at 40 °C.

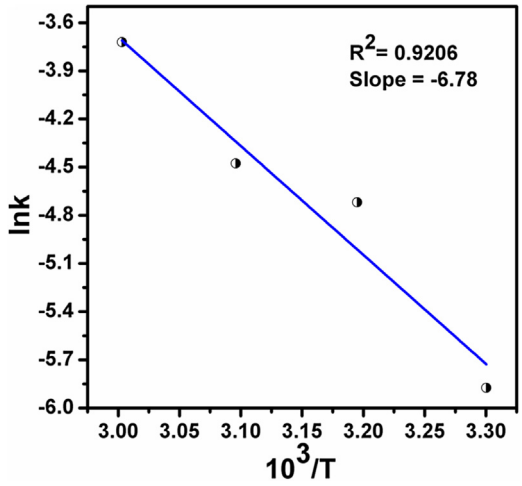

Fig. 6. Arrhenius plot for dehalogenation of **1** with PANI/Fe^0-2 catalyst at different temperatures.

3.3. Kinetics studies

To get insight of the reaction mechanism, details kinetic investigations were performed at different temperatures. In all cases, the plot of ln[A] versus time 't', depicted in Fig. 5, was fitted well with pseudo-first-order model ([A] = variable concentration (g/L) of 1-bromonaphthelene at different time). The pseudo-first-order rate constants (k) for dehalogenation of 1-bromonaphthalene and *t*-BuMgCl under standard condition at 30, 40, 50, and 60 °C were 0.00281, 0.00893, 0.01137 and 0.02421 min^{-1}, respectively, where R^2 = 0.9743–0.9977. The reaction profile diagram for substrate consumption rate and the rate of product formation is shown in Fig. 4 indicating the reductive dehalogenation reaction was kinetically facile and exhibited no additional induction period. However, the rate of catalytic efficiency of different 4-haloanisoles (Table, entries 6–8) indicated that the oxidative addition of aryl halide to catalyst is believed to be the rate determining step of proposed catalytic cycle.

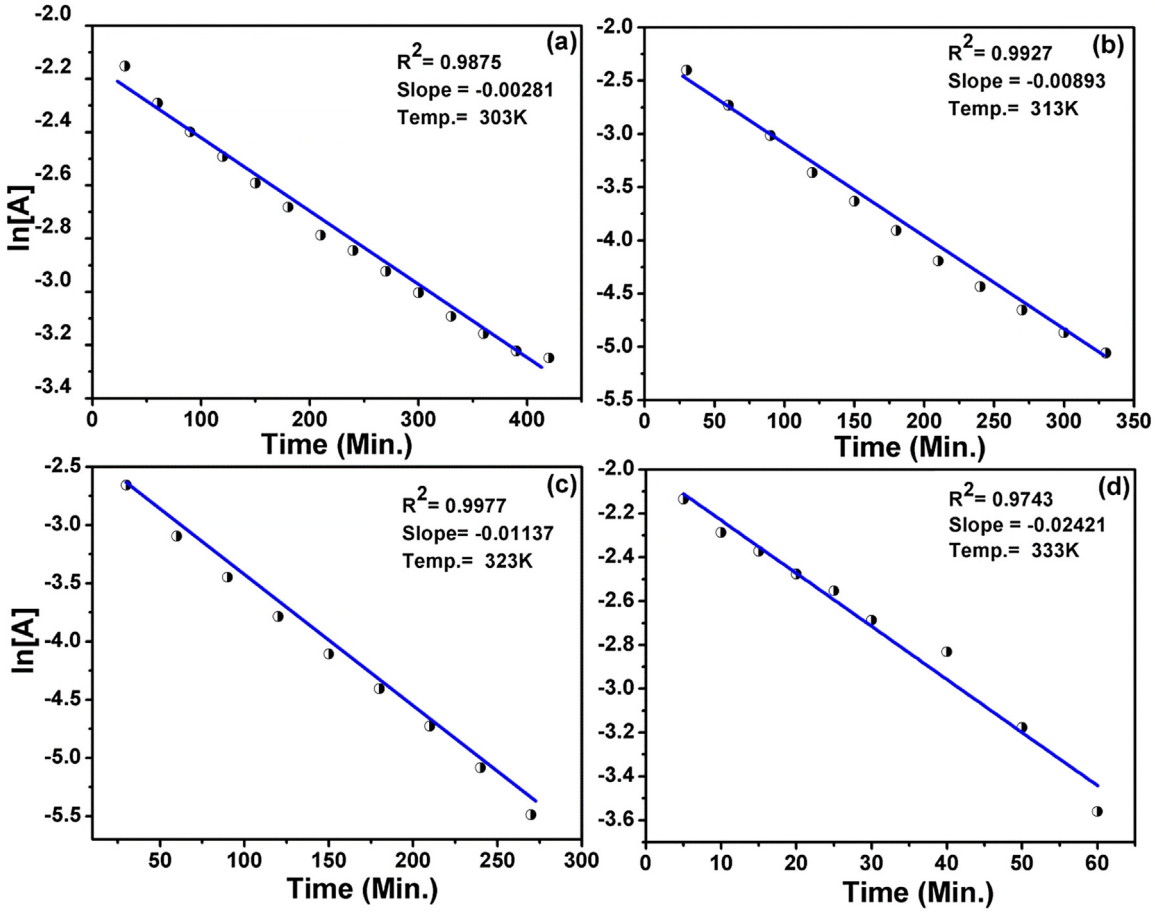

Fig. 5. Plot of ln[**A**] versus time for the debromination reaction of 1-bromonaphthalene at different temperatures [30 °C (**a**), 40 °C (**b**), 50 °C (**c**) and 60 °C (**d**)] from which rate constants (k) were calculated. [A] = variable concentration (g/L) of 1-bromonaphthalene at different time.

Table 3
Control deuteration experiments.[a]

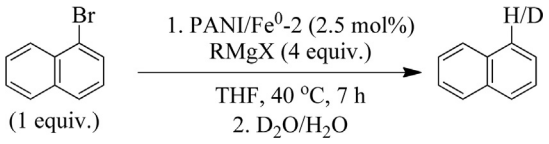

Entry	RMgX	D_2O/H_2O	Product
1.	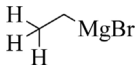	D_2O	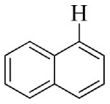
2.	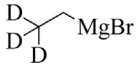	H_2O	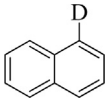
3.		H_2O	none
4.	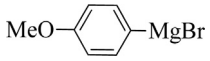	H_2O	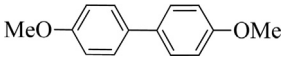

[a] Reaction condition: 1-bromonaphthalene (1 mmol), THF (2 mL), PANI/Fe^0-2 (2.5 mol%), RMgX (4 equiv.), 40 °C, 7 h.

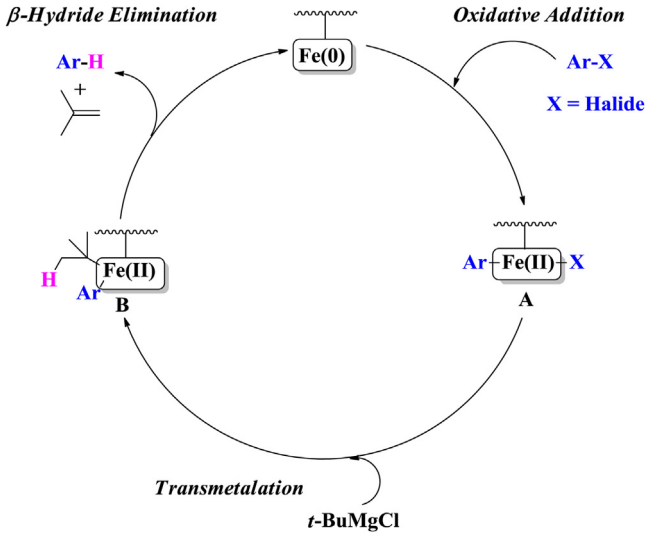

Fig. 7. Plausible mechanism for PANI/Fe^0-2 catalyzed dehalogenation.

The activation energy for the dehalogenation reaction of **1** and **2** using PANI/Fe^0-2 was calculated using Arrhenius equation at four different temperatures in the range of 30–60 °C, as shown in Fig. 6. The plot of lnk versus 10^3/T to the Arrhenius equation provided an estimated activation energy of 56.3 kJ/mol (R^2 = 0.92), which justified the catalytic reactivity of the PANI/Fe^0-2 for dehalogenation. In this regard, it is noteworthy to mention that a minor amount of reduction product (<10%) was obtained without employment of catalyst (Table 1, entry 14), which revealed a definite catalytic role of the catalyst for present transformation reaction.

3.4. Mechanistic investigation

Mechanistic investigation of dehalogenation of aryl halides using homogeneous iron catalyst was established by Czaplik and co-workers [28]. The proposed catalytic cycle for dehalogenation of aryl halide with *t*-BuMgCl is illustrated in Fig. 7. For example, initial oxidative addition of aryl halide with *t*-BuMgCl in the presence of PANI/Fe^0-2 catalyst is expected to generate intermediate **A**. Involvement of intermediate **A** with *t*-BuMgCl gives the intermediate **B** in transmetallation process and rapid β-hydride elimination afford the corresponding reduction product along with the formation of *i*-butene. However, a very small amount of cross-coupled product (<10%) was obtained with EtMgBr *via* reductive elimination step.

To support the postulated mechanism, selected experiments were performed with various Grignard reagents in the presence of PANI/Fe^0-2 catalyst. The reaction was tested using commercially available EtMgBr with **1** under standard reaction condition and quenched with D_2O (Table 3, entry 1). There is no detectable amount of deuterium incorporated in this condition. So, it was concluded that hydride source must come from β-hydrogen of complex intermediate **B**. To support the conclusion, identical reaction was examined with CD_3CH_2MgBr and quenched with H_2O (Table 3, entry 2). However, CD_3CH_2MgBr was prepared from bromoethane-2,2,2-D_3 using known method [28]. Satisfyingly, deuterium incorporated product, naphthalene-1-D, was obtained. (confirmed by ^2H NMR, see SI-G). Herein, we mentioned that naphthalene-1-D gave the chemical shift (δ) at 7.84 ppm in ^2H NMR (61.39 MHz, see SI). However, ^1H NMR chemical shift (δ) values of naphthalene-1-D [δ = 7.81-7.83 (m, 3H), 7.44-7.47 (m, 4H)] and naphthalene-2-D [δ = 7.81-7.83 (m, 4H), 7.44–7.47 (m, 3H)] were reported in literature [65]. These observations confirmed that deuterium (D) was incorporated at α-position of naphthalene from the complex **B** through β-hydride elimination process (Fig. 7). Additionally, two control reactions were done using different Grignard reagents containing no β-hydrogen and these attempts did not furnish any reduction product (Table 3, entry 3 and 4). Only 40% homo-coupling product was obtained from 4-methoxyphenyl magnesium bromide (Table 3, entry 4). The starting material, 1-bromonaphthalene, was recovered exclusively from both reaction mixtures. In addition, to test the degradation byproducts during the span of reaction, the reaction mixture was analyzed after 1 h, 2 h and 7 h using GC (see SI-I). The results confirmed that there was no degraded product observed with *t*-BuMgCl. Only dehalogenaed product was noticed in GC after 1 h, 2 h and 7 h reaction time. However, 1-Bromonaphthalene was fully converted to naphthalene after 7 h reaction time.

Table 4
Dehalogenation by three successive uses of same PANI/Fe^0-2 catalyst.[a]

Entry	Catalyst (mol%)	Time (h)	Yield (%)[b]
1st use	2.5	7	78
2nd use	2.5	16	75
3rd use	2.5	24	72

[a] Reactioncondition:1-bromonaphthalene (1 mmol), toluene (2 mL), PANI/Fe^0-2 (2.5 mol%), *t*-BuMgCl (4 equiv.), 40 °C.
[b] Isolated yield.

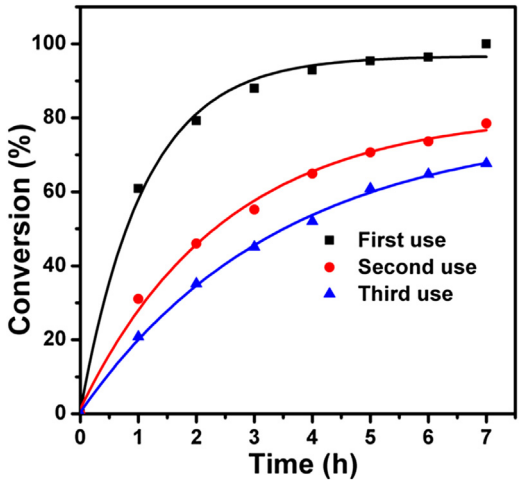

Fig. 8. Time-conversion plot of three successive uses of same PANI/Fe^0-2 catalyst.

3.5. *Re-uses of PANI/Fe^0-2 catalyst for dehalogenation*

To examine catalytic reusability, the catalyst was recovered from the reaction mixture simply by filtration after quenching with methanol and washed with acetone. After wards, catalyst sample was dried under high vacuum for 24 h at 40 °C and employed for next cycle. The process was repeated until three cycles. To accomplish complete conversion in second and third cycles, the reactions were performed for prolonged time period of 16 h and 24 h, respectively. These studies furnished the corresponding product with a yield of 72–78% (Table 4, entries 1–3). However, leaching studies (ICP-OES analysis) of liquid phase after completion of reaction revealed that 0.1 ppm Fe was leached to the solution after first cycle of the PANI/Fe^0-2 catalyst. The time-conversion plot of three consecutive uses of same catalyst was shown in Fig. 8. This attempt implied that modest deactivation of the catalyst was observed during the span of reaction time.

4. Conclusion

In summary, we successfully demonstrated the PANI/Fe^0 based catalyzed dehalogenation reaction of a variety of aryl halides with *t*-BuMgBr as a reductant under optimized reaction condition *via* β-hydride elimination. Only 2.5 mol% of PANI/Fe^0-2 catalyst was employed for this catalytic dehalogenation reaction, which is kinetically facile exhibiting activation energy of 56.3 KJ/mol. The recyclability tests of catalyst were performed up to three cycles and no significant Fe-leaching was observed after first cycle. The catalyst deactivation was observed during the course of reaction. Easy preparation of catalyst, low catalyst loading, cheap and earth abundant Fe-embedded nanocomposite material will be an alternative catalyst for dehalogenation of environmentally recalcitrant complexed halogenated aromatics.

Acknowledgements

The authors sincerely acknowledge to the University of South Africa (UNISA), the National Research Foundation (NRF), the Department of Science and Technology (DST) and the Council for Scientific and Industrial Research (CSIR), South Africa, for financial support. The characterization unit at the DST-CSIR National Centre for Nanostructured Materials is acknowledged for assisting with materials characterization.

Appendix A. Supplementary data

Supplementary data associated with this article can be found, in the online version, at http://dx.doi.org/10.1016/j.apcatb.2016.09.027.

References

[1] B.J. Alloway, D.C. Ayres, Chemical Principles of Environmental Pollution, Blackie Glasgow, 1993.
[2] M.J. Smith, S. Muller, W. Sander, G. Bucher, J. Hazard. Mater. 246–247 (2013) 154–162.
[3] J. de Boer, P.G. Wester, H.J.C. Klammer, W.E. Lewis, J.P. Boon, Nature 394 (1998) 28–29.
[4] G.W. Gribble, Chem. Soc. Rev. 28 (1999) 335–346.
[5] E.W. Schmidt, A.Y. Obraztsova, S.K. Davidson, D.J. Faulkner, M.G. Haygood, Mar. Biol. 136 (2000) 969–977.
[6] J. Luo, J. Hu, X. Wei, L. Fu, L. Li, Chemosphere 131 (2015) 17–33, and reference cited therein.
[7] P. Eriksson, E. Jakobsson, A. Fredriksson, Environ. Health Persp. 109 (2001) 903–908.
[8] P. Alvarez-Zaldivara, F. Centlera, U. Maierc, M. Thullnera, G. Imfeld, Ecol. Eng. 90 (2016) 170–179.
[9] W. Chang, C. Sun, X. Pang, H. Sheng, Y. Li, H. Ji, W. Song, C. Chen, W. Ma, J. Zhao Angew, Chem. Int. Ed. 54 (2015) 2052–2056.
[10] S.S. Gupta, M. Stadler, C.A. Noser, A. Ghosh, B. Steinho, D. Lenoir, C.P. Horwitz, K.W. Schramm, T.J. Collins, Science 296 (2002) 326–328.
[11] X. Liang, D. Fu, R. Liu, Q. Zhang, T. Zhang, X. Hu, Angew. Chem. Int. Ed. 44 (2005) 5520–5523.
[12] K.A.P. Payne, C.P. Quezada, K. Fisher, M.S. Dunstan, F.A. Collins, H. Sjuts, C. Levy, S. Hay, S.E.J. Rigby, D. Leys, Nature 517 (2015) 513–516.
[13] C. Yang, A. Kublik, C. Weidauer, B. Seiwert, L. Adrian, Environ. Sci. Technol. 49 (2015) 8497–8505.
[14] T. Weidlich, J. Oprsal, A. Krejcova, Monatsh. Chem. 146 (2015) 613–620.
[15] Y. Kuang, J. Du, R. Zhou, Z. Chen, M. Megharaj, R. Naidu, J. Colloid Interface Sci. 447 (2015) 85–91.
[16] C. Rettenmeier, H. Wadepohl, L.H. Gade, Chem. Eur. J. 20 (2014) 9657–9665.
[17] F.-L. Xue, J. Qi, P. Peng, G.-Z. Mo, Z.-Y. Wang, Lett. Org. Chem. 11 (2014) 64–79.
[18] P. Stepnicka, M. Semler, J. Demel, A. Zukal, J. Cejka, J. Mol. Catal. A: Chem. 341 (2011) 97–102.
[19] M.L. Buil, M.A. Esteruelas, S. Niembro, M. Olivan, Organometallics 29 (2010) 4375–4383.
[20] C. Huberta, E.G. Bile, A. Denicourt-Nowicki, A. Roucoux, Appl. Catal. A 394 (2011) 215–219.
[21] S. Sabater, J.A. Mata, E. Peris, Nat. Commun. 4 (2013) 1–7.
[22] J. Risse, M.A. Fernandez-Zumel, Y. Cudre, K. Severin, Org. Lett. 14 (2012) 3060–3063.
[23] C. Mukai, T. Kozaka, Y. Suzuki, I.J. Kim, Tetrahedron 60 (2004) 2497–2507.
[24] C.P. Davie, R.L. Danheiser, Angew. Chem. Int. Ed. 44 (2005) 5867–5870.
[25] P.P. Cellier, J.-F. Spindler, M. Taillefer, H.-J. Cristau, Tetrahedron Lett. 44 (2003) 7191–7195.
[26] G. Chelucci, S. Figus, J. Mol. Catal. A: Chem. 393 (2014) 191–209, and reference cited therein.
[27] L. Liua, F. Chena, F. Yanga, Y. Chenb, J. Crittenden, Chem. Eng. J. 181–182 (2012) 189–195.
[28] W.M. Czaplik, S. Grupe, M. Mayer, A.J. von Wangelin, Chem. Commun. 46 (2010) 6350–6352.
[29] Z. Zhang, Q. Shen, N. Cissoko, J. Wo, X. Xu, J. Hazard. Mater. 182 (2010) 252–258.
[30] M. Shen, W.-H. Sun, Appl. Organometal. Chem. 23 (2009) 51–54.
[31] E. Farnetti, R.D. Monte, J. Kasper, Homogeneous and Heterogeneous catalysis, in: I. Bertini (Ed.), Inorganic and Bio-Inorganic Chemistry, Vol. II, Eolss Publishers, Oxford, United Kingdom, 2007, pp. 50–87.
[32] E. Gross, J.H.-C. Liu, F.D. Toste, G.A. Somorjai, Nat. Chem. 4 (2012) 947–952, and references cited therein.
[33] Y. Zhang, X. Cui, F. Shi, Y. Deng, Chem. Rev. 112 (2012) 2467–2505.
[34] A. Grirrane, A. Corma, H. Garcia, Science 322 (2008) 1661–1664.
[35] C.A. Witham, W. Huang, C.-K. Tsung, J.N. Kuhn, G.A. Somorjai, F.D. Toste, Nat. Chem. 2 (2010) 36–41.
[36] D. Astruc, F. Lu, J.R. Aranzaes, Angew. Chem. Int. Ed. 44 (2005) 7852–7872.

[37] A.A. Toutov, W.B. Liu, K.N. Betz, A. Fedorov, B.M. Stoltz, R.H. Grubbs, Nature 518 (2015) 80–84.
[38] C. Bolm, J. Legros, J.L. Paih, L. Zani, Chem. Rev. 104 (2004) 6217–6254.
[39] J.L. Fillol, Z. Codola, I. Garcia-Bosch, L. Gomez, J.J. Pla, M. Costas, Nat. Chem. 3 (2011) 807–813.
[40] R.V. Jagadeesh, T. Stemmler, A.E. Surkus, H. Junge, K. Junge, M. Beller, Nat. Protoc. 10 (2015) 548–557.
[41] G. Cahiez, A. Moyeux, J. Buendia, C. Duplais, J. Am. Chem. Soc. 129 (2007) 13788–13789 (and reference cite therein).
[42] X. Yue, Z. Liua, Q. Zhanga, X. Li, F. Hao, J. Wei, W. Guo, Desalin. Water Treat. 57 (2016) 15190–15199.
[43] B. Haspulat, A. Gülce, H. Gülce, J. Hazard. Mater. 260 (2013) 518–526.
[44] M. Bhaumik, H.J. Choi, R.I. McCrindle, A. Maity, J. Colloid Interface Sci. 466 (2016) 442–451.
[45] M. Bhaumik, R.I. McCrindle, A. Maity, S. Agarwal, V.K. Gupta, J. Colloid Interface Sci. 425 (2014) 75–82.
[46] M. Bhaumik, R.I. McCrindle, A. Maity, Chem. Eng. J. 260 (2015) 716–729.
[47] Y.M. Abu, K. Aoki, J. Electroanal. Chem. 583 (2005) 133–139.
[48] S. de Souza, J.E.P. da Silva, S.I.C. de Torresi, M.L.A. Temperini, R.M. Torresi, Electrochem. Solid State Lett. 4 (2001) B27–B30.
[49] Q. Yi, H. Chu, M. Tang, Y. Zhang, X. Liu, Z. Zhou, H. Nie, Fuel Cells 14 (2014) 827–833.
[50] N. Daems, X. Sheng, Y. Alvarez-Gallego, I.F.J. Vankelecom, P.P. Pescarmona, Green Chem. 18 (2016) 1547–1559.
[51] C.M. Johnston, P. Zelenay, Science 332 (2011) 443–447.
[52] X.-F. Lu, X.-Y. Chen, W. Zhou, Y.X. Tong, G.R. Li, ACS Appl. Mater. Interfaces 7 (2015) 14843–14850.
[53] M.M. Bidgolia, M. Mohsennia, F.A. Boroumand, Mater. Res. Bull. 72 (2015) 29–34.
[54] D.K. Bandgar, S.T. Navale, M. Naushad, R.S. Mane, F.J. Stadler, V.B. Patil, RSC Adv. 5 (2015) 68964–68971.
[55] C.T. Lin, C.W. Huang, IEEE Sens. J. 10 (2010) 1142–1146.
[56] B. Sim, H.S. Chae, H. Choi, eXPRESS Polym. Lett. 9 (2015) 736–743.
[57] Y. Chen, S. Lu, W. Liu, J. Han, Colloid Polym. Sci. 293 (2015) 2301–2309 (and reference cited therein).
[58] M. Bhaumik, C. Noubactep, V.K. Gupta, R.I. McCrindle, A. Maity, Chem. Eng. J. 271 (2015) 135–146 (and reference cited therein).
[59] Q.S. Gao, S.N. Wang, Y. Tang, C. Giordano, Chem. Commun. 48 (2012) 260–262.
[60] J. Yin, X. Xiang, L. Xiang, X. Zhao, J. Mater. Chem. 20 (2010) 7096–7099.
[61] R. Dev, N. Mukherjee, S. Ahammed, B.C. Ranu, Chem. Commun. 48 (2012) 7982–7984.
[62] P. Scherrer, Göttinger Nachrichten, Math Phys. 2 (1918) 98–100.
[63] Y.P. Sun, X.Q. Li, J. Cao, W.X. Zhang, H.P. Wang, Adv. Colloid Interface Sci. 120 (2006) 47–56.
[64] S.R. Kanel, B. Manning, L. Charlet, H. Choi, Environ. Sci. Technol. 39 (2005) 1291–1298.
[65] Y. Miura, H. Oka, E. Yamano, M. Morita, J. Org. Chem. 62 (1997) 1188–1190.